PCCP

PAPER

Cite this: *Phys. Chem. Chem. Phys.*, 2021, **23**, 18506

Directed gas-phase preparation of the elusive phosphinosilylidyne ($SiPH_2$, X^2A'') and *cis*/*trans* phosphinidenesilyl (HSiPH; X^2A') radicals under single-collision conditions†

Chao He,[a] Shane J. Goettl,[a] Zhenghai Yang,[a] Srinivas Doddipatla,[a] Ralf I. Kaiser,*[a] Mateus Xavier Silva[b] and Breno R. L. Galvão*[b]

Received 22nd June 2021,
Accepted 12th August 2021

DOI: 10.1039/d1cp02812j

rsc.li/pccp

The reaction of the D1-silylidyne radical (SiD; $X^2\Pi$) with phosphine (PH_3; X^1A_1) was conducted in a crossed molecular beams machine under single collision conditions. Merging of the experimental results with *ab initio* electronic structure and statistical Rice–Ramsperger–Kassel–Marcus (RRKM) calculations indicates that the reaction is initiated by the barrierless formation of a van der Waals complex (**i0**) as well as intermediate (**i1**) formed *via* the barrierless addition of the SiD radical with its silicon atom to the non-bonding electron pair of phosphorus of the phosphine. Hydrogen shifts from the phosphorous atom to the adjacent silicon atom yield intermediates **i2a**, **i2b**, **i3**; unimolecular decomposition of these intermediates leads eventually to the formation of *trans*/*cis*-phosphinidenesilyl (HSiPH, **p2**/**p4**) and phosphinosilylidyne ($SiPH_2$, **p3**) *via* hydrogen deuteride (HD) loss (experiment: 80 ± 11%, RRKM: 68.7%) and D-*trans*/*cis*-phosphinidenesilyl (DSiPH, **p2′**/**p4′**) plus molecular hydrogen (H_2) (experiment: 20 ± 7%, RRKM: 31.3%) through indirect scattering dynamics *via* tight exit transition states. Overall, the study reveals branching ratios of **p2**/**p4**/**p2′**/**p4′** (*trans*/*cis* HSiPH/DSiPH) to **p3** ($SiPH_2$) of close to 4 : 1. The present study sheds light on the complex reaction dynamics of the silicon and phosphorous systems involving multiple atomic hydrogen migrations and tight exit transition states, thus opening up a versatile path to access the previously elusive phosphinidenesilyl and phosphinosilylidyne doublet radicals, which represent potential targets of future astronomical searches toward cold molecular clouds (TMC-1), star forming regions (Sgr(B2)), and circumstellar envelopes of carbon rich stars (IRC + 10216).

1. Introduction

Since the pioneering isolation of the methyleneamidogen radical (H_2CN, $^2B_2$, **1**) in solid argon in 1962 by Cochran *et al.*,[1] the structural isomers *trans*-iminomethyl (*trans*-HCNH, $^2A'$, **2**), *cis*-iminomethyl (*cis*-HCNH, $^2A'$, **3**), and aminomethylidyne (CNH_2, $^2B_2$, **4**) along with the isovalent homologues silylenephosphino (H_2SiP, $^2B_2$, **5**), *trans*-phosphinidenesilyl (*trans*-HSiPH, $^2A'$, **6**), phosphinosilylidyne ($SiPH_2$, $^2A''$, **7**), and *cis*-phosphinidenesilyl (*cis*-HSiPH, $^2A'$, **8**) have been of considerable interest to the physical (organic), material, astrochemistry, and theoretical chemistry communities from the fundamental points of views of electronic structure and chemical bonding (Scheme 1).[2–28] The methyleneamidogen radical (H_2CN, $^2B_2$, **1**) was detected *via* the 1_{01}–0_{00} transition in the Taurus Molecular Cloud (TMC-1) and through the 2_{02}–1_{01} transition in Sagittarius B2 (Sgr B2).[11] This radical was predicted to exist in the circumstellar envelope of the carbon-rich star IRC + 10216; a possible formation pathway could be the hitherto unstudied reaction of $N(^4S) + CH_3 \rightarrow H_2CN + H$.[12,13] The methyleneamidogen radical (H_2CN, $^2B_2$, **1**) has been also identified as a reactive intermediate in the combustion of hexahydro-1,3,5-trinitro-1,3,5-triazine ($(CH_2NNO_2)_3$, RDX) and octahydro-1,3,5,7-tetranitro-1,3,5,7-tetrazine ($(CH_2NNO_2)_4$, HMX).[5–8] To elucidate the molecular and electronic structure, multiple spectroscopic experiments were designed.[14–18] As early as 1968, Ogilvie and coworker detected the electronic absorption spectra of H_2CN (**1**) at 281–285 nm in the gas phase with radicals prepared by flash photolysis of $(CH_2N)_2$.[14] Jacox reported the ultraviolet (UV) and infrared (IR) spectra of H_2CN (**1**) along with a vibrational assignment of the structured $^2A_1$–$^2B_2$ band.[15] The microwave spectrum of methyleneamidogen radical (H_2CN, **1**) in the $^2B_2$ ground electronic state was also collected.[16] Multiple calculations revealed that the C_{2v} symmetric radical methyleneamidogen radical (H_2CN, $^2B_2$, **1**) represents the most stable of the four isomers (**1**, **2**, **3**, **4**).[2,4,9,19–21] The results reveal

[a] Department of Chemistry, University of Hawai'i at Manoa, Honolulu, Hawaii, 96822, USA. E-mail: ralfk@hawaii.edu

[b] Centro Federal de Educação Tecnológica de Minas Gerais, CEFET-MG, Av. Amazonas 5253, 30421-169 Belo Horizonte, Minas Gerais, Brazil. E-mail: brenogalvao@gmail.com

† Electronic supplementary information (ESI) available: Fig. S1–S3 and Tables S1–S6. See DOI: 10.1039/d1cp02812j

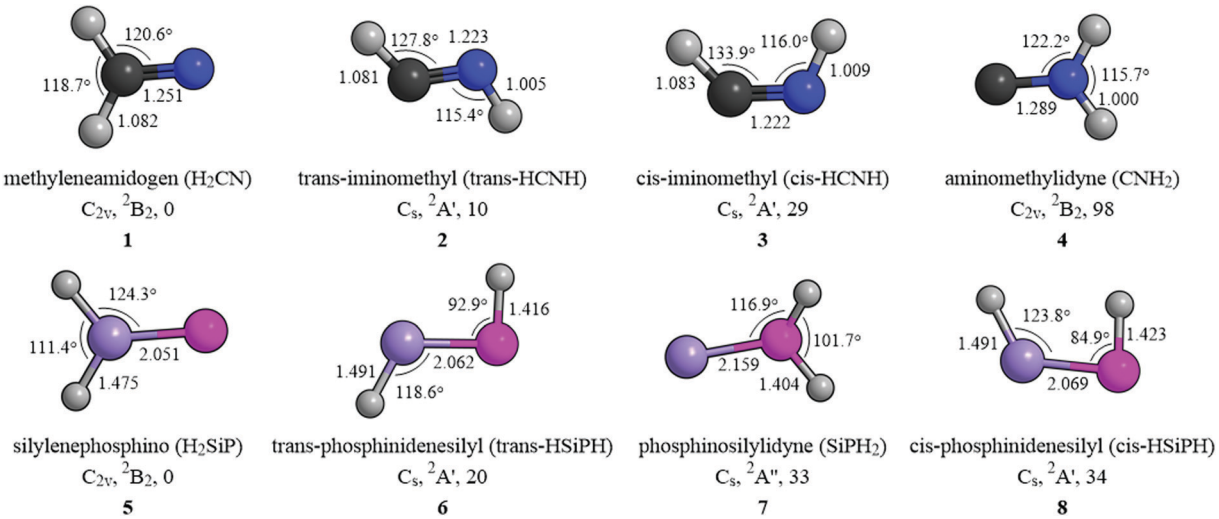

Scheme 1 Molecular geometries of isovalent species of methyleneamidogen (H_2CN), iminomethyl (HCNH), and aminomethylidyne (CNH_2) along with relative energies (kJ mol^{-1}), point groups, and electronic ground state wave functions; bond distances (Å) and bond angles (°) are also provided. Atoms are colored as follows: carbon, black; nitrogen, blue; hydrogen, grey; silicon, purple; phosphorus, pink.

that the *trans*-HCNH (**2**), *cis*-HCNH (**3**), and CNH_2 (**4**) isomers are less stable than planar H_2CN (**1**) by 10, 29, and 98 kJ mol^{-1}, respectively.[2,4,9,21] Raksit *et al.* reported the first observation of HCNH (**2**, **3**) radical in the lab by neutralized ion beam spectroscopy.[3] The aminomethylidyne (CNH_2, **4**) radical, which is the simplest iminium species, was identified *via* the thermal decomposition of hydrogen cyanide (HCN), azomethane ($CH_3N_2CH_3$), and methylamine (CH_3NH_2).[22–25]

Compared to the H_2CN system **1**, **2**, **3**, and **4**, gas phase studies on the isovalent H_2SiP system [H_2SiP (**5**), *trans*-HSiPH (**6**), $SiPH_2$ (**7**), and *cis*-HSiPH (**8**)], in which the main group XIV and XV elements carbon and nitrogen are replaced by the isovalent silicon and phosphorus counterparts, are remarkably lacking.[26–28] Iwata and coworkers computed the H_2SiP potential energy surface (PES) utilizing the G2 approach as well as a hybrid DFT (B3LYP/6-311G**) method.[28] The C_{2v} symmetric H_2SiP (**5**) represents the global minimum; this structure is best described as a molecule holding a Si–P double bond along with a lone-pair as well as a radical center located on the phosphorus atom. The second low-lying isomer *trans*-HSiPH (**6**) and its conformer *cis*-HSiPH (**8**) are 23 and 40 kJ mol^{-1} higher than H_2SiP (**5**), respectively. The conformers *trans*-HSiPH (**6**) and *cis*-HSiPH (**8**) are connected *via* a low barrier of 49 kJ mol^{-1} relative to *trans*-HSiPH (**6**). Therefore, the facile interconversion of *trans*-HSiPH (**6**) and *cis*-HSiPH (**8**) isomers suggests the difficulty to distinguish them experimentally. The $SiPH_2$ radical (**7**) is predicted to be less stable than H_2SiP (**5**) by 28–41 kJ mol^{-1}. Baboul *et al.*[27] optimized the geometries of **5**, **6**, **7**, and **8** at the MP2/6-31G(d) level of theory and the relative energies were calculated by the G2 method. The structures of H_2SiP (**5**), *trans*-HSiPH (**6**), and *cis*-HSiPH (**8**) are planar along with a Si–P double bond. The *trans*-HSiPH (**6**), $SiPH_2$ (**7**), *cis*-HSiPH (**8**) molecules are less stable than H_2SiP (**5**) by 16, 38, 21 kJ mol^{-1}, respectively.[26,27] The differences of molecular structures and chemical bonding of the H_2CN system (**1**, **2**, **3**, **4**) and the isovalent H_2SiP species (**5**, **6**, **7**, **8**) are reflected in the bond lengths and angles. The Si–P bond lengths of from 2.051 to 2.159 Å in H_2SiP isomers (**5**, **6**, **7**, **8**) are longer than the C–N bond length of from 1.222 to 1.289 Å in the isovalent H_2CN radicals (**1**, **2**, **3**, **4**) (Scheme 1). Further, the H_2SiP molecules (**5**, **6**, **7**, **8**) hold Si–H bond lengths of 1.475 to 1.491 Å compared to the shorter C–H bond lengths of 1.082 to 1.083 Å in the H_2CN analogs (**1**, **2**, **3**, **4**); also, the P–H bond lengths of 1.404 to 1.423 Å in H_2SiP isomers (**5**, **6**, **7**, **8**) are longer than the N–H bond length of 1.000 to 1.009 Å in the H_2CN species (**1**, **2**, **3**, **4**). The H–Si–P angle (124.3°) in H_2SiP (**5**) agrees well with the corresponding H–C–N angle (120.6°) in H_2CN (**1**), whereas the Si–P–H angle (116.9°) in $SiPH_2$ (**7**) is smaller than the C–N–H angle (122.2°) in CNH_2 (**4**). For the conformer pairs *trans*/*cis*-HSiPH (**6**, **8**) and *trans*/*cis*-HCNH (**2**, **3**), the Si–P–H angles in *trans*/*cis*-HSiPH (**6**, **8**) of 84.9° to 92.9° are smaller than the corresponding C–N–H angles in *trans*/*cis*-HCNH (**2**, **3**) of 116.0° and 115.4°, respectively; this suggests an sp^2-hybridization of the nitrogen atom and hence a H–N bond with an sp^2 orbital at the nitrogen atom, but an H–P bond involving a non-hybridized p orbital at the phosphorus atom, which would give an ideal H–P–Si bond angle of 90°. However, as of now, none of these H_2SiP molecules (**5**, **6**, **7**, **8**) has been identified experimentally.

The aforementioned compilation reveals that the formation mechanisms of the H_2SiP isomers (**5**, **6**, **7**, **8**) are far from being resolved. Herein, we access the $SiPDH_3$ PES *via* the bimolecular reaction of the D1-silylidyne radical (SiD; $X^2\Pi$) with phosphine (PH_3; X^1A_1). By merging the crossed molecular beam data with electronic structure calculations, we demonstrate that at least *trans*-phosphinidenesilyl (HSiPH), D-*trans*-phosphinidenesilyl (DSiPH), phosphinosilylidyne ($SiPH_2$), *cis*-phosphinidenesilyl (HSiPH), and D-*cis*-phosphinidenesilyl (DSiPH) can be formed under single collision conditions. Phosphine (PH_3; X^1A_1) has been identified in circumstellar envelopes of IRC + 10216 and toward star-forming regions like SgrB2;[29] the silylidyne radical

(SiH; $X^2\Pi$) may be inferred to exist in star forming regions such as Orion Kleinmann-Low nebula;[30] therefore, a synthesis of *trans*/*cis*-phosphinidenesilyl (*trans*/*cis*-HSiPH, **6**/**8**) and phosphinosilylidyne ($SiPH_2$, **7**) in these extraterrestrial environments is predicted.

2. Methods

2.1. Experimental

The gas-phase reaction of the D1-silylidyne radical (SiD; $X^2\Pi$) with phosphine (PH_3; X^1A_1) was conducted under single-collision conditions using a universal crossed molecular beams machine at the University of Hawaii.[31–36] In the primary source chamber, a pulsed supersonic D1-silylidyne radicals was produced *in situ* by laser ablation of a rotating silicon rod (Si; 99.999%; Goodfellow Cambridge Limited) at 266 nm, 6 ± 1 mJ pulses (Spectra-Physics Quanta-Ray Pro 270 Nd:YAG laser; 30 Hz) and seeding the ablated species in a gas mixture of deuterium gas (D_2; 99.999% purity; ≥99.75% D atom; Linde) and neon (Ne; 99.999%; Airgas) with a ratio of 1 : 1 and a total pressure of 4 atm. According to the isotopic abundances of silicon (92.23% ^{28}Si; 4.67% ^{29}Si; 3.1% ^{30}Si) and that a fraction of the D1-silylidyne radical to atomic silicon in the primary beam was 10 ± 3%, the D1-silylidyne beam was optimized at a unique m/z = 31 (^{29}SiD) for intensity; no higher molecular weight silicon–deuterium bearing species were observed. The supersonic beam of D1-silylidyne radicals passed through a skimmer and was velocity-selected by a four-slot chopper wheel resulting a well-defined peak velocity (v_p) and speed ratio (S) of 1253 ± 30 m s^{-1} and 6.7 ± 2.0 (Table 1), respectively. It should be noted that the supersonic beam also contains ground state atomic silicon (Si(^{3}P)); in the selected part of the beam, a D1-silylidyne to atomic silicon ratio of 0.12 ± 0.02 : 1 was determined, *i.e.* a fraction of about 10%. In the secondary source chamber, the pulsed supersonic beam of phosphine (≥99.9995%; Matheson Tri-Gas) was regulated at 550 Torr along with v_p of 805 ± 9 m s^{-1} and S of 12.4 ± 0.1 (Table 1). The phosphine molecular beam crossed perpendicularly with the primary beam D1-silylidyne radicals in the main chamber yields a collision energy (E_C) of (17.7 ± 0.7) kJ mol^{-1} and a center of mass angle (Θ_{CM}) of (36.1 ± 1.0)°. Note that even if the primary beam contained D1-silylidyne radicals in the $A^2\Delta$ excited state formed initially in the ablation center, taking into account of their short lifetime of around 500 ns,[37] they will decay to the ground state $X^2\Pi$ during the travel time of about 36 μs to the interaction region in the main chamber.

The neutral reaction products entering the detector were ionized by an electron impact ionizer (80 eV, 2 mA),[38] then filtered according to the mass-to-charge ratio (m/z) utilizing a quadrupole mass spectrometer (QMS, Extrel, QC 150) coupled with a 2.1 MHz oscillator, and eventually recorded by a Daly-type ion counter.[39] The detector is housed within a triply differentially pumped and rotatable chamber that allows the collection of angularly-resolved time-of-flight (TOF) spectra in the plane defined by both reactant beams. To obtain the information on the reaction dynamics, a forward-convolution method was used to transform the laboratory frame (LAB) data into the center of mass frame (CM),[40,41] which represents an iterative method whereby user-defined CM translational energy $P(E_T)$ and angular $T(\theta)$ flux distributions are varied iteratively until a best fit of the laboratory-frame TOF spectra and angular distributions are achieved.[42,43] These functions comprise the reactive differential cross-section $I(\theta,u)$, which is taken to be separable into its CM scattering angle θ and CM velocity u components, $I(u,\theta) \sim P(u) \times T(\theta)$.[44–46] The error ranges of the $P(E_T)$ and $T(\theta)$ functions are determined within the 1σ limits of the corresponding laboratory angular distribution and beam parameters (beam spreads, beam velocities) while maintaining a good fit of the laboratory TOF spectra.

Table 1 Peak velocities (v_p) and speed ratios (S) of the D1-silylidyne (SiD), and phosphine (PH_3) beams along with the corresponding collision energy (E_C) and center-of-mass angle (Θ_{CM})

Beam	v_p (m s^{-1})	S	E_C (kJ mol^{-1})	Θ_{CM} (degree)
SiD ($X^2\Pi$)	1253 ± 30	6.7 ± 2.0		
PH_3 (X^1A_1)	805 ± 9	12.4 ± 0.1	17.7 ± 0.7	36.1 ± 1.0

2.2. Computational

The electronic structure calculations reported here were performed using GAMESS-US[47] and MOLPRO[48] packages. Initial exploration of the potential energy surface (PES) was carried out employing density functional theory (DFT)[49] and the M06-2X[50] exchange and correlation functional along with the cc-pV(T+d)Z basis set.[51–53] All calculations employ restricted wavefunctions in order to avoid spin contamination and no symmetry restrictions were imposed in any optimization. Vibrational analysis was carried out for all stationary points found at the M06-2X/cc-pV(T+d)Z level and both non-deuterated and singly-deuterated cases were taken into account. The isotopic substitution considered one deuterium at each possible position for every structure obtained in this work from the SiD ($X^2\Pi$) plus PH_3 (X^1A_1) reaction. Structures that corresponded to energy minima were confirmed by presenting only real vibrational frequencies, while transition states (TSs) were confirmed by the presence of a single imaginary frequency. Intrinsic reaction coordinate (IRC) calculations starting from each TS found were performed to ensure the correct connection paths. Further single point energy calculations at the explicitly correlated CCSD(T)-F12/cc-pVQZ-F12[54,55] level were performed over the geometries optimized at the M06-2X/cc-pV(T+d)Z level in order to provide higher accuracy energy values. This methodology is referred here as CCSD(T)-F12/cc-pVQZ-F12//M06-2X/cc-pV(T+d)Z + ZPE(M06-2X/cc-pV(T+d)Z), and generally shows an accuracy better than 10 kJ mol^{-1}. For discussion purposes, we report the calculation results with this error margin. All structures and parameters are reported in Table S6 (ESI†).

3. Results

3.1. Laboratory frame

For the reactive scattering experiments of the D1-silylidyne radical (SiD; $X^2\Pi$) with phosphine (PH_3; X^1A_1), it is important

to consider the natural isotope abundances of silicon [^{28}Si (92.2%), ^{29}Si (4.7%), ^{30}Si (3.1%)]. This might complicate the interpretation of the data of the atomic (H, D) and/or molecular hydrogen loss (H_2, HD). Second, besides the D1-silylidyne radical, the primary beam also contains ground state atomic silicon Si(^3P_j), which reacts with phosphine to form HPSi isomers plus molecular hydrogen (reaction (1)); note that the endoergic atomic hydrogen loss channel to any H_2PSi isomer was closed in the Si–PH_3 system.[56] Recall that in the Si–PH_3 system, reactive scattering signal was collected for from m/z = 65 to 60 with signals at m/z = 62 and 61 recorded at levels of (3 ± 3)% and (7 ± 3)% compared to m/z = 60 (Table S1, ESI†). No signal at m/z = 65 to 63 is detectable in the Si–PH_3 system. Considering the silicon and D1-silylidyne reactants, feasible mass combinations for the Si(^{3}P)–PH_3 (reaction (1)) and SiD–PH_3 systems (reactions (2)–(5)) are summarized in Tables S2 and S3, respectively (ESI†). Based on the results and discussion below, reaction signal of the SiD–PH_3 system can be distinguished from that of the Si–PH_3 system due to distinct laboratory angular distributions along with distinct ratio in mass-to-charge ratios (Table S1, ESI†). This methodology has been successfully adopted to extract the distinct chemical dynamics of the Si–D_2S/H_2S[57] *versus* SiD–D_2S/H_2S[58] and Si–SiH_4[59] *versus* SiD–SiH_4/SiD_4 systems.[60]

In detail, reactive scattering signal was explored from m/z = 60 to m/z = 65 (Table S1, ESI†) to probe the atomic hydrogen loss ($^{30}SiPDH_2^+$, m/z = 65; $^{29}SiPDH_2^+$, m/z = 64; $^{28}SiPDH_2^+$, m/z = 63) (reaction (2)), the atomic deuterium loss ($^{30}SiPH_3^+$, m/z = 64; $^{29}SiPH_3^+$, m/z = 63; $^{28}SiPH_3^+$, m/z = 62) (reaction (3)), the molecular hydrogen loss ($^{30}SiPDH^+$, m/z = 64; $^{29}SiPDH^+$, m/z = 63; $^{28}SiPDH^+$, m/z = 62) (reaction (4)), and hydrogen deuteride loss ($^{30}SiPH_2^+$, m/z = 63; $^{29}SiPH_2^+$, m/z = 62; $^{28}SiPH_2^+$, m/z = 61) (reaction (5)). The following conclusions can be drawn from the laboratory data alone.

$$Si + PH_3 \rightarrow SiPH + H_2 \quad (1)$$

$$SiD + PH_3 \rightarrow SiPDH_2 + H \quad (2)$$

$$SiD + PH_3 \rightarrow SiPH_3 + D \quad (3)$$

$$SiD + PH_3 \rightarrow SiPDH + H_2 \quad (4)$$

$$SiD + PH_3 \rightarrow SiPH_2 + HD \quad (5)$$

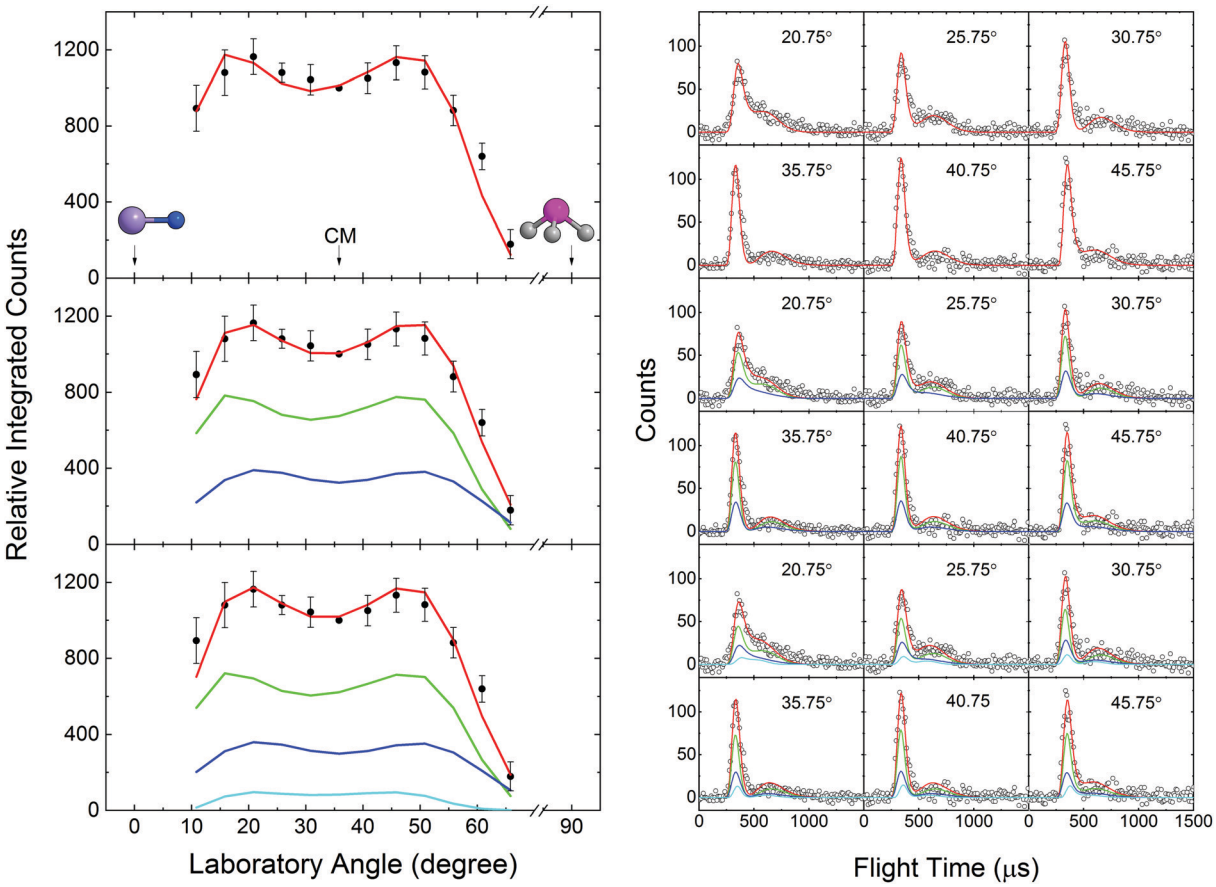

Fig. 1 Laboratory angular distribution (left) and time-of-flight (TOF) spectra (right) recorded at m/z = 61 for the reaction of the D1-silylidyne radical (SiD; $X^2\Pi$) with phosphine (PH_3; X^1A_1). The data were fit with a single channel (top), with two channels (middle), and with three channels (bottom): (i) ^{28}SiD (30 amu) + PH_3 (34 amu) → $^{28}SiPH_2$ (61 amu) + HD (3 amu) (green), (ii) ^{29}Si (29 amu) + PH_3 (34 amu) → ^{29}SiPH (61 amu) + H_2 (2 amu) (blue), and (iii) dissociative electron impact ionization of the m/z = 62 ($^{28}SiPDH^+$) formed in the reaction ^{28}SiD (30 amu) + PH_3 (34 amu) → ^{28}SiPDH (62 amu) + H_2 (2 amu) (light blue). CM represents the center-of-mass angle, and 0° and 90° define the directions of the D1-silylidyne and phosphine beams, respectively. The black circles depict the experimental data, colored lines the fits (red corresponding to the total fit), and error bars the 1σ standard deviation.

First, no signal was observable at m/z = 65 and m/z = 64 (Table S1, ESI†) revealing that the absence of any adducts ($^{29}SiPDH_3^+$, m/z = 65; $^{28}SiPDH_3^+$, m/z = 64). Likewise, potential contributions of the atomic hydrogen/deuterium loss and molecular hydrogen elimination pathway – if present in the SiD/PH_3 system – are below the detection limits; therefore, at least for these channels, ^{29}SiD and ^{30}SiD do not contribute to any reactive scattering signal. Second, signal was observed from m/z = 63 to 60 (Table S1, ESI†). Signal at m/z = 63 is unique to the SiD–PH_3 system as no signal at m/z = 63 was observed in the Si–PH_3 system; this signal could originate from four sources: (i) molecular hydrogen loss channel ($^{29}SiPDH^+$, m/z = 63; reaction (4)), (ii) hydrogen deuteride loss channel ($^{30}SiPH_2^+$, m/z = 63; reaction (5)), (iii) atomic deuterium loss ($^{29}SiPH_3^+$, m/z = 63; reaction (3)), and (iv) atomic hydrogen loss ($^{28}SiPDH_2^+$, m/z = 63; reaction (2)). Ion counts at m/z = 63 and 62 were accumulated at fraction of 4 ± 1% and 9 ± 1% compared to m/z = 61 (Fig. S1 and Table S1, ESI†). Recall that in the Si–PH_3 system, ion counts at m/z = 62 and 61 were collected at levels of 3 ± 3% and 7 ± 3%, respectively, compared to m/z = 60 (Table S1, ESI†). The comparison of both data sets indicates that m/z = 61 represents the main reactive scattering signal in SiD–PH_3 system. This can be accounted for through the reaction of the D1-silylidyne radical (SiD; $X^2\Pi$) with phosphine (PH_3) forming $SiPH_2$ isomer(s) predominantly *via* the reaction of ^{28}SiD along with the emission of hydrogen deuteride (HD; 3 amu) leading to signal at m/z = 61 ($SiPH_2$); molecular hydrogen loss (H_2; 2 amu) yielding signal at m/z = 62 (SiPDH) likely accounts for a minor fraction of the ion counts in SiD–PH_3 reaction. Since signal of m/z = 63 and m/z = 62 are significantly weaker compared with that of m/z = 61 and m/z = 60 and these time-of-flight (TOF) spectra are identical after scaling (Fig. S1, ESI†), TOF spectra and the full laboratory angular distributions were extracted at m/z = 61 and m/z = 60 (Fig. 1 and 2), respectively. Both laboratory angular distributions are rather broad, almost forward–backward symmetric with regard to the center-of-mass (CM) angle of 36°, and are spread over scattering angles from at least 10.8° to 65.8°. These results indicate that the reaction proceeds *via* indirect scattering dynamics involving the existence of $SiPDH_3$ intermediate(s). Additional information can be extracted by examining the Newton diagrams for the hydrogen deuteride loss channel for the SiD–PH_3 system as well as for the molecular hydrogen loss pathway of the Si–PH_3 reaction (Fig. S3, ESI†). The radii of the recoil circles represent the maximum CM velocity of the reactively scattered heavy products; each circle spans an angular range in which the corresponding product is expected to be observed by the detector. The laboratory angular distribution at m/z = 60 has a similar shape as m/z = 61 (Fig. S2, ESI†), but shows a noticeable broadening at higher angles; this pattern is expected for the HD loss channels in the SiD–PH_3 system.

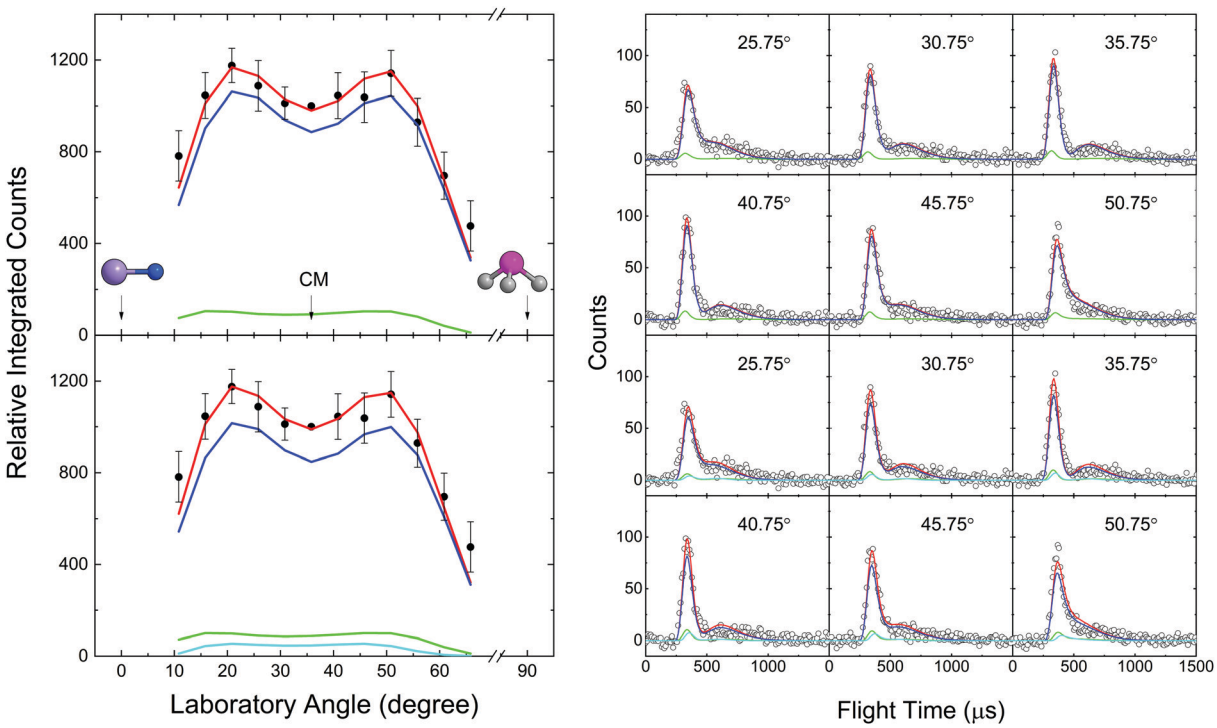

Fig. 2 Laboratory angular distribution (left) and time-of-flight spectra (right) recorded at m/z = 60 for the reaction of the D1-silylidyne radical (SiD; $X^2\Pi$) with phosphine (PH_3; X^1A_1) exploiting a two-channel fit (top) and a three-channel fit (bottom): (i) ^{28}Si (28 amu) + PH_3 (34 amu) → ^{28}SiPH (60 amu) + H_2 (2 amu) (blue), (ii) dissociative electron impact ionization of the neutral products at m/z = 61 formed *via* ^{28}SiD (30 amu) + PH_3 (34 amu) → $^{28}SiPH_2$ (61 amu) + HD (3 amu) (green), and (iii) dissociative electron impact ionization of the m/z = 62 ($^{28}SiPDH^+$) formed in the reaction ^{28}SiD (30 amu) + PH_3 (34 amu) → ^{28}SiPDH (62 amu) + H_2 (2 amu) (light blue). CM represents the center-of-mass angle, and 0° and 90° define the directions of the D1-silylidyne and phosphine beams, respectively. The black circles depict the experimental data, colored lines the fits (red corresponding to the total fit), and error bars the 1σ standard deviation.

3.2. Center-of-mass frame

To elucidate the chemical dynamics of the bimolecular reactions of the SiD–PH_3 system, the experimental data were transformed from the laboratory into the CM reference frame to obtain the CM translational energy $P(E_T)$ and angular $T(\theta)$ flux distributions (Fig. 3 and 4).[42]

3.2.1. *m/z* = 61. The TOFs and laboratory angular distribution at $m/z = 61$ (Fig. 1) could be replicated through a single channel fit corresponding to the reaction ^{28}SiD (30 amu) + PH_3 (34 amu) → $^{28}SiPH_2$ (61 amu) + HD (3 amu) (Fig. 1 (top)). The $P(E_T)$ (Fig. 3) shows a maximum translational energy of $E_{max} = 90 \pm 19$ kJ mol^{-1}; for those molecules born without internal excitation, the maximum energy release represents the sum of the reaction energy plus the collision energy thus revealing a reaction energy of -72 ± 19 kJ mol^{-1}. The distribution further reveals a distribution maximum of 55 kJ mol^{-1} suggesting a tight exit barrier from the decomposing $SiPDH_3$ intermediate(s) to form the $SiPH_2$ plus HD products with a repulsive energy release and significant 'reorganization' of the electron density from the decomposing complex to the final products. Further, the average translational energy of the products was derived to be 56 ± 12 kJ mol^{-1} indicating that $62 \pm 14\%$ of the available energy is transformed into the translational degrees of freedom of the products. Finally, the $T(\theta)$ (Fig. 3) depicts non-zero intensity over the complete scattering range from 0° to 180°; this finding is indicative of indirect scattering dynamics *via* the formation of $SiPH_2$ complex(es); the forward-backward symmetry of $T(\theta)$ implies that the lifetime of the decomposing $SiPDH_3$ complex is longer than the rotational period(s).[61]

However, $m/z = 61$ could also be a contributor from the Si–PH_3 reaction,[56] *i.e.* the formation of ^{29}SiPH (61 amu) plus molecular hydrogen (2 amu). To objectively account for this possibility, we also attempted to fit the laboratory angular distribution at $m/z = 61$ with two channels (Fig. 1 (middle)) with the CM functions of the molecular hydrogen loss channel for the Si–PH_3 system extracted from He *et al.*[56] Here, we could add a contribution from the Si–PH_3 reaction of up to $33 \pm 5\%$. This fraction agrees well with a predicted fraction of $39 \pm 4\%$ considering a D1-silylidyne to atomic silicon ratio of $0.12 \pm 0.02:1$ and the silicon isotopes contributing to $m/z = 61$ (^{28}Si (92.2%), ^{29}Si (4.7%)) (Tables S1–S3, ESI†).

Finally, $m/z = 61$ could also be a contributor from dissociative electron impact ionization of the $m/z = 62$ ($^{28}SiPDH^+$) formed *via* the ^{28}SiD (30 amu) + PH_3 (34 amu) → ^{28}SiPDH (62 amu) + H_2 (2 amu) reaction. Therefore, a third fit (Fig. 1, bottom) was attempted utilizing three channels: (i) ^{28}SiD (30 amu) + PH_3 (34 amu) → $^{28}SiPH_2$ (61 amu) + HD (3 amu), (ii) ^{29}Si (29 amu) + PH_3 (34 amu) → ^{29}SiPH (61 amu) + H_2 (2 amu), and (iii) dissociative

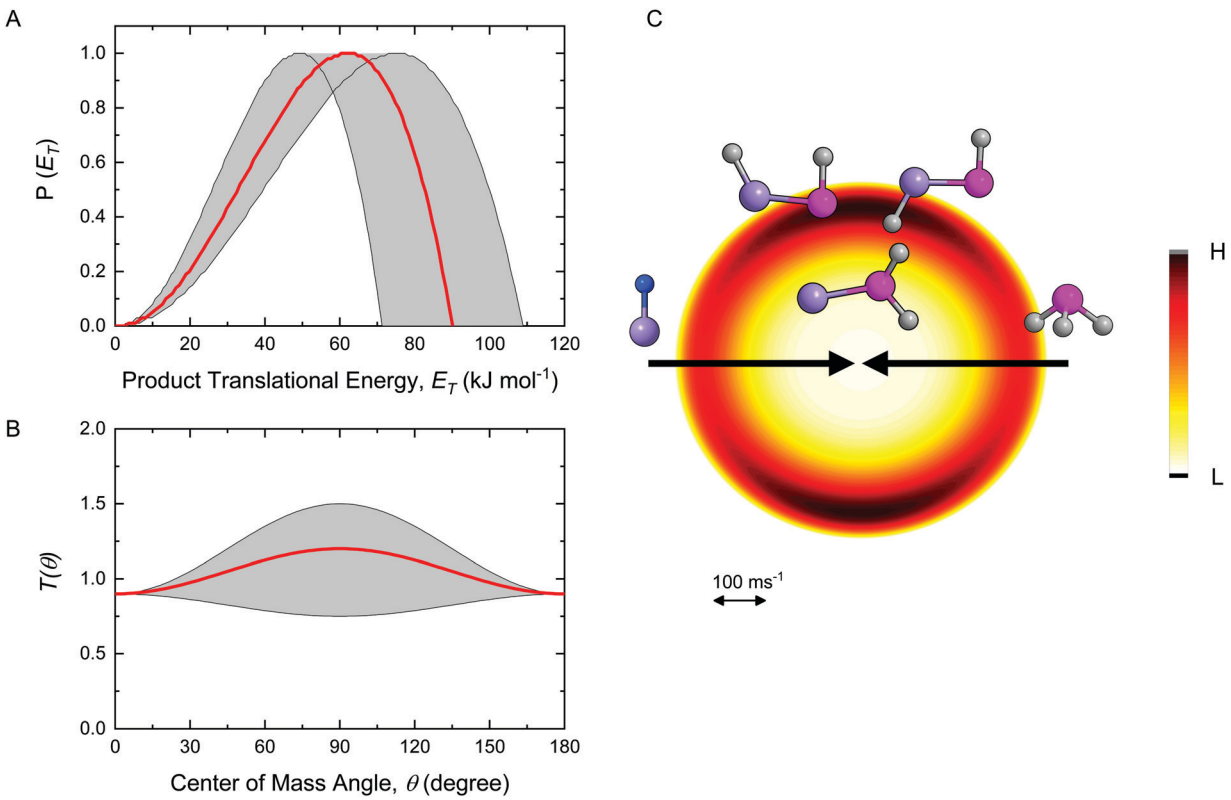

Fig. 3 CM translational energy flux distribution (A), CM angular flux distribution (B), and the top view of the flux contour map (C) leading to the formation of *trans*-phosphinidenesilyl (*trans*-HSiPH), phosphinosilylidyne ($SiPH_2$), and *cis*-phosphinidenesilyl (*cis*-HSiPH). Shaded areas indicate the acceptable upper and lower error limits, while the red solid lines define the best fits. The flux contour map represents the flux intensity of the reactively scattered heavy products as a function of the CM scattering angle (θ) and product velocity (u). The color bar manifests the flux gradient from high (H) intensity to low (L) intensity. Colors of the atoms: silicon, purple; phosphorus, pink; hydrogen, gray; and deuterium, blue.

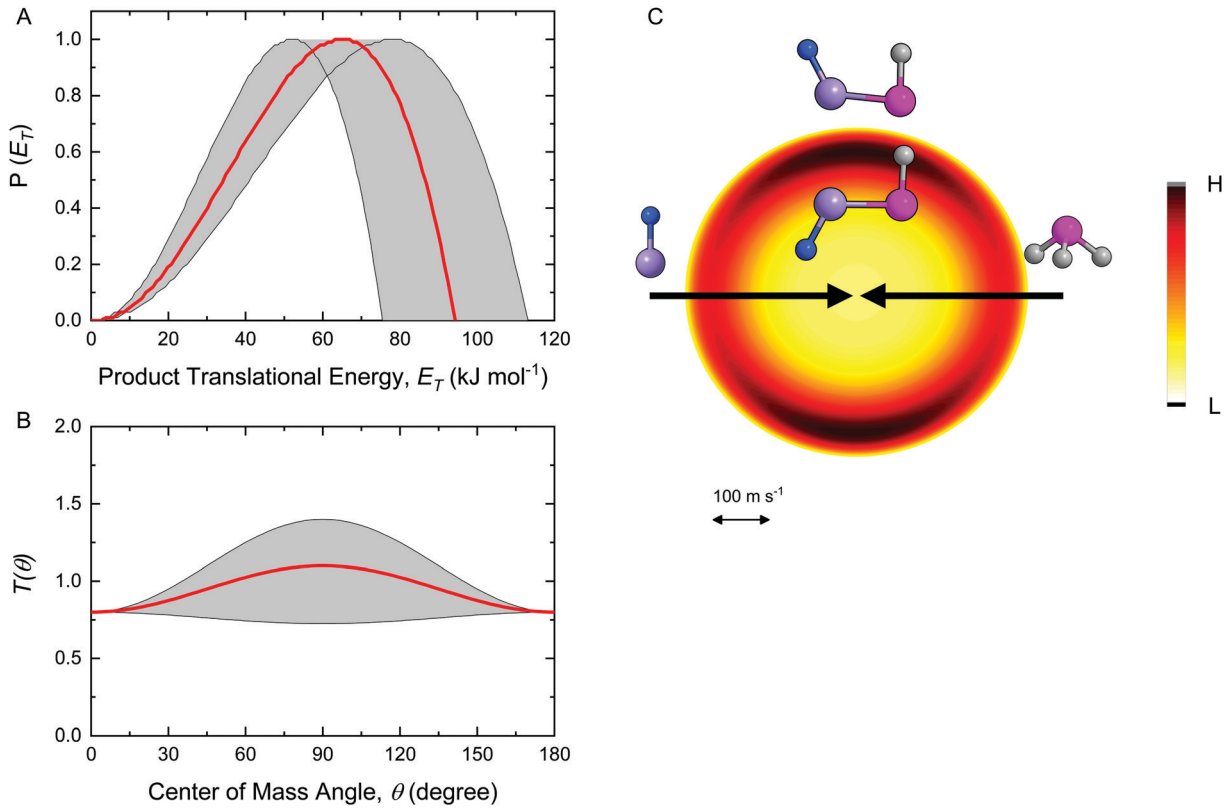

Fig. 4 CM translational energy flux distribution (A), CM angular flux distribution (B), and the top view of the flux contour map (C) leading to the formation of D-*trans*-phosphinidenesilyl (*trans*-DSiPH) and D-*cis*-phosphinidenesilyl (*cis*-DSiPH). Shaded areas indicate the acceptable upper and lower error limits, while the red solid lines define the best fits. The flux contour map represents the flux intensity of the reactively scattered heavy products as a function of the CM scattering angle (θ) and product velocity (u). The color bar manifests the flux gradient from high (H) intensity to low (L) intensity. Colors of the atoms: silicon, purple; phosphorus, pink; hydrogen, gray; and deuterium, blue.

electron impact ionization of the m/z = 62 (^{28}SiPDH$^+$) formed in the reaction ^{28}SiD (30 amu) + PH_3 (34 amu) → ^{28}SiPDH (62 amu) + H_2 (2 amu). A three-channel fit could reproduce the laboratory data with branching ratios of 57 ± 8%, 29 ± 6%, and 14 ± 5%, respectively (Fig. 1 (bottom)) suggesting a minor contribution of the third channel – if any. The corresponding center-of-mass functions of this channel are displayed in Fig. 4. For the ^{28}SiD (30 amu) + PH_3 (34 amu) → ^{28}SiPDH (62 amu) + H_2 (2 amu) reaction, a maximum translational energy (E_{max}) of 94 ± 19 kJ mol^{-1} was derived from the $P(E_T)$. Considering $E_{max} = E_C - \Delta_r G$, a reaction energy was computed to be −76 ± 19 kJ mol^{-1} for products born without internal excitation. The $P(E_T)$ distribution reveals a most probable E_T located at 58 kJ mol^{-1} suggesting a tight exit barrier from the decomposing $SiPDH_3$ intermediate(s) to form the final products SiPDH plus H_2. Further, the average translational energy of the products was deduced to be 58 ± 12 kJ mol^{-1} indicating that 62 ± 13% of the available energy is disposed into the translational degrees of freedom of the products. Finally, the forward–backward symmetry of $T(\theta)$ (Fig. 4) along with non-zero intensity over the complete scattering range from 0° to 180° once again suggests the indirect scattering dynamics *via* the formation of SiPDH complex(es) and the reaction proceeds through a long-lived $SiPDH_3$ complex.[61]

In summary, the data of the SiD–PH_3 system provided evidence on the existence of at least the $SiPH_2$ (61 amu) plus HD (3 amu) and possibly the SiPDH (62 amu) plus H_2 (2 amu) channel with a maximum fraction of the latter of 20 ± 7%. It should be noted that atomic hydrogen or deuterium loss channels could not fit the laboratory data. Considering the computed potential energy surface (Fig. 4), these pathways are endoergic by 10–12 ± 10 kJ mol^{-1} and hence likely do not compete with the exoergic molecular HD/H_2 channels. An in-depth discussion is provided below.

3.2.2. *m/z* = 60. Signal at m/z = 60 could originated from the reaction ^{28}Si (28 amu) + PH_3 (34 amu) → ^{28}SiPH (60 amu) + H_2 (2 amu) (channel i). However, m/z = 60 could also be a contributor from dissociative electron impact ionization of the neutral products at m/z = 61 formed *via* ^{28}SiD (30 amu) + PH_3 (34 amu) → $^{28}SiPH_2$ (61 amu) + HD (3 amu) (channel ii). This two-channel fit utilizing both contributions could reproduce the experimental data with branching ratios of 91 ± 5% and 9 ± 8%, for channel i and ii, respectively (Fig. 2, top). Finally, we also explored if a third channel - dissociative electron impact ionization of the neutral products at m/z = 62 (^{28}SiPDH$^+$) formed in the reaction ^{28}SiD (30 amu) + PH_3 (34 amu) → ^{28}SiPDH (62 amu) + H_2 (2 amu) – could be implemented. The fits suggest only minor contributions – if at all (Fig. 2, bottom).

4. Discussion

In case of polyatomic reactions involving third row atoms, it is always beneficial to combine the experimental results with electronic structure calculations to provide further information on the underlying reaction mechanism(s) in the SiD–PH_3 system (Fig. 5). Overall, four intermediates and multiple isomerization and exit transition states *via* hydrogen deuteride emission ($SiPH_2$; **p1**, **p2**, **p3**, **p4**), molecular hydrogen loss (SiPDH; **p1′**, **p2′**, **p4′**), atomic deuterium emission (H_2SiPH; **p5**), and atomic hydrogen loss (HDSiPH; **p5′**) were identified. The reaction products for the H_2/HD channels were revealed to be exoergic between -89 ± 10 to 53 ± 10 kJ mol^{-1}, whereas the H/D loss channels were endoergic between 10 ± 10 to 70 ± 10 kJ mol^{-1}. In detail, the reaction between the D1-silylidyne radical (SiD) and phosphine (PH_3) is initiated by the initial formation of a weakly bound (20 kJ mol^{-1}) van der Waals complex **i0** or through a barrierless addition of the D1-silylidyne radical to the non-bonding electron pair of the phosphorus atom forming a covalently bound intermediate with a phosphorus–silicon single bond **i1**. At a collision energy of 17.7 kJ mol^{-1}, **i0** can isomerize *via* a barrier of only 12 kJ mol^{-1} *via* insertion of the silicon atom of the SiD radical into one of the three chemically equivalent phosphorus–hydrogen single bonds of phosphine forming intermediate **i2a** ($HDSiPH_2$). Intermediate **i1** can undergo a hydrogen shift from the phosphorus to the silicon atom *via* a barrier of 77 kJ mol^{-1} yielding intermediate **i2b** ($HDSiPH_2$). Both **i2a** and **i2b** are connected through a low lying transition state only 7 kJ mol^{-1} above **i2a** *via* rotation around the P–H single bond. What is the ultimate fate of these reaction intermediates? Intermediate **i2a** may undergo unimolecular decomposition *via* hydrogen deuteride loss leading to product **p3** (phosphinosilylidyne, $SiPH_2$, $^2A''$) in an overall exoergic reaction ($\Delta_r G = -55 \pm 10$ kJ mol^{-1}). This intermediate can also isomerize through a hydrogen migration from the phosphorus to the silicon atom forming intermediate **i3**. This process is linked to a barrier of 98 kJ mol^{-1}. At a collision energy of 17.7 kJ mol^{-1}, intermediate **i3** is expected to decompose predominantly *via* hydrogen deuteride loss to form *cis*-phosphinidenesilyl (*cis*-HSiPH, **p4**, $^2A'$, $\Delta_r G = -55 \pm 10$ kJ mol^{-1}) or through molecular hydrogen loss leading to D-*cis*-phosphinidenesilyl (*cis*-DSiPH, **p4′**, $^2A'$, $\Delta_r G = -53 \pm 10$ kJ mol^{-1}); the atomic deuterium/hydrogen loss channels to silylenephosphine (H_2SiPH, **p5**, $^1A'$, $\Delta_r G = 12 \pm 10$ kJ mol^{-1}) and D-silylenephosphine (HDSiPH, **p5′**, $^1A'$, $\Delta_r G = 10 \pm 10$ kJ mol^{-1}), respectively, are less competitive. Intermediate **i2a** ($HDSiPH_2$) on the other hand can undergo hydrogen deuteride and also molecular hydrogen loss to *trans*-phosphinidenesilyl (*trans*-HSiPH, **p2**, $^2A'$, $\Delta_r G = -67 \pm 10$ kJ mol^{-1}) and D-*trans*-phosphinidenesilyl (*trans*-DSiPH, **p2′**, $^2A'$, $\Delta_r G = -69 \pm 10$ kJ mol^{-1}), respectively. The atomic hydrogen loss to

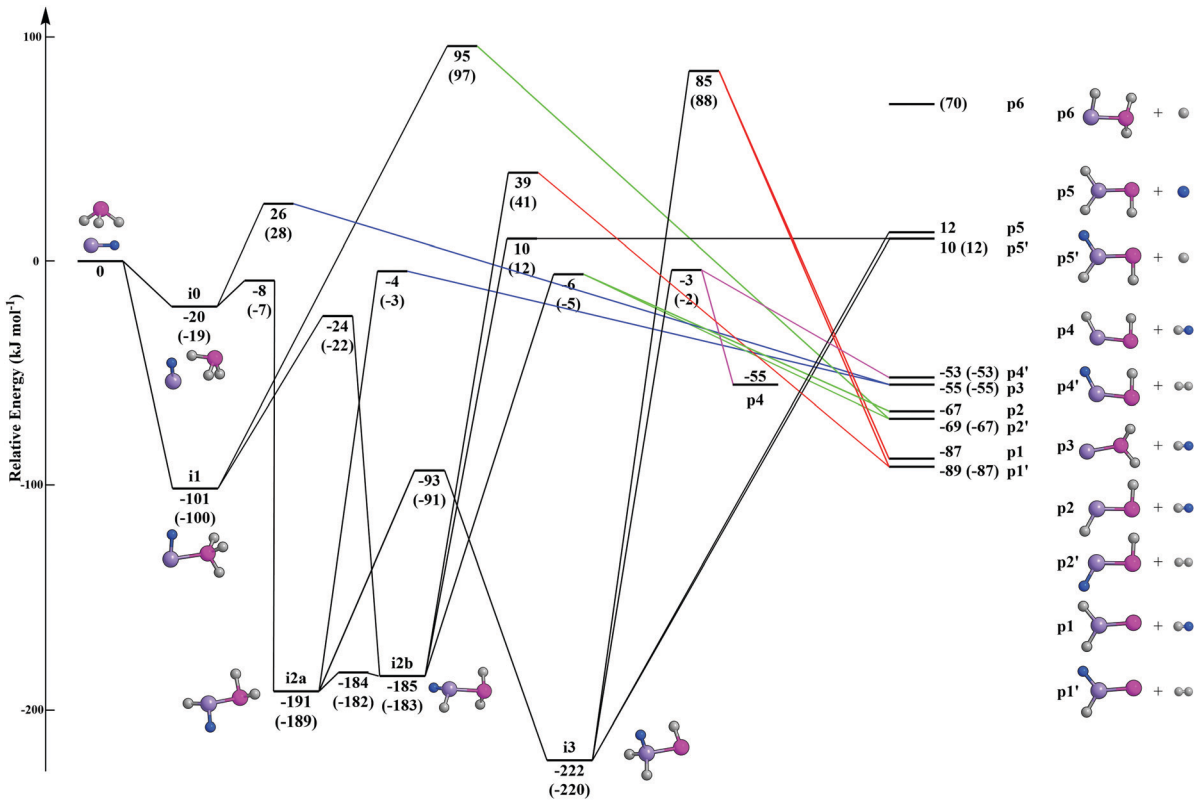

Fig. 5 Potential energy diagram of the reaction of the D1-silylidyne radical (SiD; $X^2\Pi$) with phosphine (PH_3; X^1A_1) calculated at the CCSD(T)-F12/cc-pVQZ-F12//M06-2X/cc-pV(T+d)Z + ZPE(M06-2X/cc-pV(T+d)Z) level of theory. The energies are shown in kJ mol^{-1} with respect to the energy of the separated reactants, and calculations for the non-deuterated system shown in parentheses. Atoms are colored as follows: silicon, purple; hydrogen, gray; deuterium, blue; and phosphorus, pink. Cartesian coordinates and normal modes are compiled in Tables S6 (ESI†).

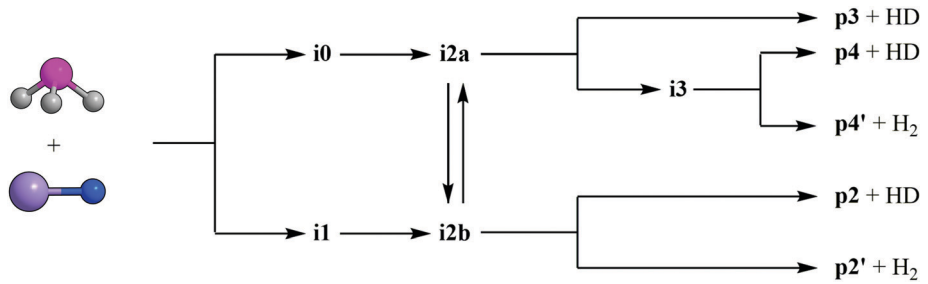

Fig. 6 Compilation of dominating reaction pathway in the reaction of D-silylidyne (SiD) with phosphine (PH_3).

D-silylenephosphine (HDSiPH, **p5′**, $^1A'$, $\Delta_r G = 10 \pm 10$ kJ mol^{-1}) is less competitive. It is important to note that the thermodynamically most stable products D-silylenephosphino (HDSiP, **p1′**, $^2B_2$, $\Delta_r G = -89 \pm 10$ kJ mol^{-1}) and silylenephosphino (H_2SiP, **p1**, $^2B_2$, $\Delta_r G = -87 \pm 10$ kJ mol^{-1}) cannot be accessed; their formation would involve the decomposition of intermediate **i3**, which has to pass a transition state located 85/88 kJ mol^{-1} above the energy of the separated reactants; this energy is well above the collision energy of 17.7 kJ mol^{-1}. Overall, the molecular hydrogen and hydrogen deuteride loss pathways can be compiled *via* Fig. 6. Therefore, we can conclude that at least *trans*-phosphinidenesilyl (**p2**), D-*trans*-phosphinidenesilyl (**p2′**), phosphinosilylidyne (**p3**), *cis*-phosphinidenesilyl (**p4**), and D-*cis*-phosphinidenesilyl (**p4′**) can be formed under our experimental conditions. These pathways involve all tight exit transition states ranging between 50 and 73 kJ mol^{-1} above the energies of the separated products; recall that tight exit transition state(s) were predicted based on the derived center-of-mass translational energy distribution.

Finally, we explored the branching ratios of the individual products **p1–p4** utilizing statistical Rice–Ramsperger–Kassel–Marcus (RRKM) theory (Tables S4 and S5, ESI†) under the assumption of a complete energy randomization.[62,63] Two sets of calculations were conducted starting with each a 100% population of **i0** and **i1**. Since **i0** and **i1** isomerize to **i2a** and **i2b**, respectively, and the low lying barrier of isomerization between both latter intermediates provide an equal population, the results of both sets of RRKM calculations are identical. Overall, the study predicts *trans*-phosphinidenesilyl (**p2**), D-*trans*-phosphinidenesilyl (**p2′**), phosphinosilylidyne (**p3**), *cis*-phosphinidenesilyl (**p4**), and D-*cis*-phosphinidenesilyl (**p4′**) contribute 15.8%, 15.8%, 21.7%, 31.2%, and 15.6% at $E_C = 17.7$ kJ mol^{-1}, respectively. Hence, for the SiD + PH_3 system, the HD loss channels (**p2**, **p3**, and **p4**) supplies 68.7%, whereas the H_2 emission products (**p2′**, **p4′**) yields lower fractions of 31.3%. Recall that, the results section reveals the existence of a dominant $SiPH_2$ (61 amu) + HD (3 amu) loss channel and a minor SiPDH (62 amu) + H_2 (2 amu) pathway with overall branching ratios of 80 ± 11%, and 20 ± 7%. Therefore, the RRKM results match our experimental findings very well. Although the contribution of the lower energy isomers cannot be quantified experimentally, the branching ratios of these isomers were predicted by statistical RRKM calculation.

5. Conclusion

Our crossed molecular beams experiment of the D1-silylidyne radical (SiD; $X^2\Pi$) with phosphine (PH_3; X^1A_1) merged with electronic structure and statistical calculations provided persuasive evidence on the dominating hydrogen deuteride channel (experiment: 80 ± 11%, RRKM: 68.7%) along with molecular hydrogen emission pathways (experiment: 20 ± 7%, RRKM: 31.3%) leading to *trans*/*cis*-phosphinidenesilyl (**p2**/**p4**), D-*trans*/*cis*-phosphinidenesilyl (**p2′**/**p4′**), and phosphinosilylidyne (**p3**) *via* indirect scattering dynamics through long-lived $SiPDH_3$ complexes. The reaction is initiated *via* two barrierless entrance channel involving the formation of a van der Waals complex **i0** and an addition intermediate ($DSiPH_3$, **i1**), which eventually isomerize to **i2a** and **i2b**, respectively; both latter intermediates isomerize rapidly through rotation around the silicon–phosphorus single bond. These intermediates undergo molecular hydrogen/hydrogen deuteride loss through tight exit transition states or isomerize *via* hydrogen shift to intermediate **i3** (DH_2SiPH) prior to unimolecular decomposition *via* molecular hydrogen/hydrogen deuteride loss in overall exoergic reactions (−89 to −53 kJ mol^{-1}). Finally, the first preparation and detection of (partially deuterated) previously elusive phosphinidenesilyl (HSiPH, $^2A'$) and phosphinosilylidyne ($SiPH_2$, $^2A''$) doublet radicals opens up their astronomical detection toward interstellar and/or circumstellar environments, where silylidyne and phosphine reactants are abundant such as around the circumstellar envelope of IRC + 10216 and toward star-forming regions like SgrB2.

Conflicts of interest

The authors declare no competing financial interest.

Acknowledgements

This experimental work was supported by the U.S. National Science Foundation (NSF) under Award CHE-1853541 the University of Hawaii. Financial support from Coordenação de Aperfeiçoamento de Pessoal de Nível Superior – Brasil (CAPES) – Finance Code 001 and Conselho Nacional de Desenvolvimento Científico e Tecnológico (CNPq) are also acknowledged.

References

1 E. L. Cochran, F. J. Adrian and V. A. Bowers, *J. Chem. Phys.*, 1962, **36**, 1938–1942.
2 F. Holzmeier, M. Lang, K. Hader, P. Hemberger and I. Fischer, *J. Chem. Phys.*, 2013, **138**, 214310.
3 A. B. Raksit, D. M. Hudgins, S. Buchau and R. F. Porter, *Rapid Commun. Mass Spectrom.*, 1987, **1**, 57–59.
4 E. Correa, W. B. da Silva, P. R. P. Barreto and A. F. Albernaz, *J. Mol. Model.*, 2017, **23**, 169.
5 M. H. Alexander, P. J. Dagdigian, M. E. Jacox, C. E. Kolb, C. F. Melius, H. Rabitz, M. D. Smooke and W. Tsang, *Prog. Energy Combust. Sci.*, 1991, **17**, 263–296.
6 G. F. Adams and R. W. Shaw Jr, *Annu. Rev. Phys. Chem.*, 1992, **43**, 311–340.
7 X. Zhao, E. J. Hintsa and Y. T. Lee, *J. Chem. Phys.*, 1988, **88**, 801–810.
8 C. F. Melius, *Chemistry and physics of energetic materials*, Springer, 1990, pp. 51–78.
9 N. R. Brinkmann, S. S. Wesolowski and H. F. Schaefer III, *J. Chem. Phys.*, 2001, **114**, 3055–3064.
10 J. M. Jasinski, B. S. Meyerson and B. A. Scott, *Annu. Rev. Phys. Chem.*, 1987, **38**, 109–140.
11 M. Ohishi, D. McGonagle, W. M. Irvine, S. Yamamoto and S. Saito, *Astrophys. J.*, 1994, **427**, L51–L54.
12 T. J. Millar and E. Herbst, *Astron. Astrophys.*, 1994, **288**, 561–571.
13 T. J. Millar, E. Herbst and R. P. A. Bettens, *Mon. Not. R. Astron. Soc.*, 2000, **316**, 195–203.
14 J. F. Ogilvie and D. G. Horne, *J. Chem. Phys.*, 1968, **48**, 2248–2256.
15 M. E. Jacox, *J. Phys. Chem.*, 1987, **91**, 6595–6600.
16 S. Yamamoto and S. Saito, *J. Chem. Phys.*, 1992, **96**, 4157–4162.
17 D. C. Cowles, M. J. Travers, J. L. Frueh and G. B. Ellison, *J. Chem. Phys.*, 1991, **94**, 3517–3528.
18 M. Pettersson, J. Lundell, L. Khriachtchev and M. Räsänen, *J. Chem. Phys.*, 1998, **109**, 618–625.
19 B. Jiang and H. Guo, *J. Chem. Phys.*, 2013, **139**, 224310.
20 X. Wang and J. M. Bowman, *J. Chem. Theory Comput.*, 2013, **9**, 901–908.
21 R. A. Bair and T. H. Dunning Jr, *J. Chem. Phys.*, 1985, **82**, 2280–2294.
22 D. Jentz, M. Trenary, X. D. Peng and P. Stair, *Surf. Sci.*, 1995, **341**, 282–294.
23 D. Jentz, H. Celio, P. Mills and M. Trenary, *Surf. Sci.*, 1995, **341**, 1–8.
24 D. Jentz, P. Mills, H. Celio, M. Belyansky and M. Trenary, *J. Chem. Phys.*, 1996, **105**, 3250–3257.
25 D. Jentz, P. Mills, H. Celio and M. Trenary, *Surf. Sci.*, 1996, **368**, 354–360.
26 M. R. Zachariah and C. F. Melius, *J. Phys. Chem. A*, 1997, **101**, 913–918.
27 A. G. Baboul and H. B. Schlegel, *J. Am. Chem. Soc.*, 1996, **118**, 8444–8451.
28 J. Hrušák, D. Schröder, H. Schwarz and S. Iwata, *Bull. Chem. Soc. Jpn.*, 1997, **70**, 777–787.
29 M. Agúndez, J. Cernicharo, L. Decin, P. Encrenaz and D. Teyssier, *Astrophys. J.*, 2014, **790**, L27.
30 P. Schilke, D. J. Benford, T. R. Hunter, D. C. Lis and T. G. Phillips, *Astrophys. J., Suppl. Ser.*, 2001, **132**, 281.
31 R. I. Kaiser, P. Maksyutenko, C. Ennis, F. Zhang, X. Gu, S. P. Krishtal, A. M. Mebel, O. Kostko and M. Ahmed, *Faraday Discuss.*, 2010, **147**, 429–478.
32 N. Balucani, O. Asvany, R. I. Kaiser and Y. Osamura, *J. Phys. Chem. A*, 2002, **106**, 4301–4311.
33 R. I. Kaiser, A. M. Mebel, A. H. H. Chang, S. H. Lin and Y. T. Lee, *J. Chem. Phys.*, 1999, **110**, 10330–10344.
34 R. I. Kaiser, D. Stranges, H. M. Bevsek, Y. T. Lee and A. G. Suits, *J. Chem. Phys.*, 1997, **106**, 4945–4953.
35 F. Stahl, P. von Ragué Schleyer, H. F. Bettinger, R. I. Kaiser, Y. T. Lee and H. F. Schaefer III, *J. Chem. Phys.*, 2001, **114**, 3476–3487.
36 F. Stahl, P. V. R. Schleyer, H. F. Schaefer III and R. I. Kaiser, *Planet. Space Sci.*, 2002, **50**, 685–692.
37 W. Bauer, K. H. Becker, R. Düren, C. Hubrich and R. Meuser, *Chem. Phys. Lett.*, 1984, **108**, 560–561.
38 G. O. Brink, *Rev. Sci. Instrum.*, 1966, **37**, 857–860.
39 N. R. Daly, *Rev. Sci. Instrum.*, 1960, **31**, 264–267.
40 P. S. Weiss, PhD thesis, University of California, 1986.
41 M. F. Vernon, PhD thesis, University of California, 1983.
42 R. I. Kaiser, Y. T. Lee and A. G. Suits, *J. Chem. Phys.*, 1996, **105**, 8705–8720.
43 R. I. Kaiser, D. Stranges, Y. T. Lee and A. G. Suits, *J. Chem. Phys.*, 1996, **105**, 8721–8733.
44 R. I. Kaiser, C. Ochsenfeld, D. Stranges, M. Head-Gordon and Y. T. Lee, *Faraday Discuss.*, 1998, **109**, 183–204.
45 X. Gu, Y. Guo, F. Zhang, A. M. Mebel and R. I. Kaiser, *Faraday Discuss.*, 2006, **133**, 245–275.
46 A. M. Mebel and R. I. Kaiser, *Int. Rev. Phys. Chem.*, 2015, **34**, 461–514.
47 M. W. Schmidt, K. K. Baldridge, J. A. Boatz, S. T. Elbert, M. S. Gordon, J. H. Jensen, S. Koseki, N. Matsunaga, K. A. Nguyen, S. Su, T. L. Windus, M. Dupuis and J. A. Montgomery, *J. Comput. Chem.*, 1993, **14**, 1347–1363.
48 H.-J. Werner, P. J. Knowles, G. Knizia, F. R. Manby, M. Schütz, P. Celani, W. Györffy, D. Kats, T. Korona, R. Lindh, A. Mitrushenkov, G. Rauhut, K. R. Shamasundar, T. B. Adler, R. D. Amos, A. Bernhardsson, A. Berning, D. L. Cooper, J. O. Deegan, A. J. Dobbyn, F. Eckert, E. Goll, C. Hampel, A. Hesselmann, G. Hetzer, T. Hrenar, G. Jansen, C. Köppl, Y. Liu, A. W. Lloyd, R. A. Mata, A. J. May, S. J. McNicholas, W. Meyer, M. E. Mura, A. Nicklass, D. P. O'Neill, P. Palmieri, D. Peng, K. Pflüger, R. Pitzer, M. Reiher, T. Shiozaki, H. Stoll, A. J. Stone, R. Tarroni, T. Thorsteinsson and M. Wang, *MOLPRO, Version 2015.1, A Package of Ab Initio Programs*, University of Cardiff, Cardiff, UK, 2015. http://www.molpro.net.
49 W. Kohn and L. J. Sham, *Phys. Rev.*, 1965, **140**, A1133.
50 Y. Zhao and D. G. Truhlar, *Theor. Chem. Acc.*, 2008, **120**, 215–241.
51 T. H. Dunning Jr, K. A. Peterson and A. K. Wilson, *J. Chem. Phys.*, 2001, **114**, 9244–9253.
52 T. H. Dunning Jr, *J. Chem. Phys.*, 1989, **90**, 1007–1023.
53 R. A. Kendall, T. H. Dunning Jr and R. J. Harrison, *J. Chem. Phys.*, 1992, **96**, 6796–6806.

54 T. B. Adler, G. Knizia and H.-J. Werner, *J. Chem. Phys.*, 2007, **127**, 221106.
55 G. Knizia, T. B. Adler and H.-J. Werner, *J. Chem. Phys.*, 2009, **130**, 054104.
56 C. He, Z. Yang, S. Doddipatla, L. Zhao, S. Goettl, R. I. Kaiser, M. X. Silva and B. R. L. Galvão, *J. Phys. Chem. Lett.*, 2021, **12**, 2489–2495.
57 S. Doddipatla, C. He, S. J. Goettl, R. I. Kaiser, B. R. L. Galvão and T. J. Millar, *Sci. Adv.*, 2021, **7**, eabg7003.
58 S. J. Goettl, S. Doddipatla, Z. Yang, C. He, R. I. Kaiser, M. X. Silva, B. R. L. Galvão and T. J. Millar, *Phys. Chem. Chem. Phys.*, 2021, **23**, 13647–13661.
59 T. Yang, B. B. Dangi, R. I. Kaiser, K. H. Chao, B. J. Sun, A. H. H. Chang, T. L. Nguyen and J. F. Stanton, *Angew. Chem., Int. Ed.*, 2017, **56**, 1264–1268.
60 Z. Yang, B.-J. Sun, C. He, S. Goettl, Y.-T. Lin, A. H. H. Chang and R. I. Kaiser, *J. Phys. Chem. A*, 2021, **125**, 2472–2479.
61 W. B. Miller, S. A. Safron and D. R. Herschbach, *Discuss. Faraday Soc.*, 1967, **44**, 108–122.
62 J. I. Steinfeld, J. S. Francisco and W. L. Hase, *Chemical Kinetics and Dynamics*, Prentice Hall, Englewood Cliffs, New Jersey, 1982.
63 V. V. Kislov, T. L. Nguyen, A. M. Mebel, S. H. Lin and S. C. Smith, *J. Chem. Phys.*, 2004, **120**, 7008–7017.